ACS central science

http://pubs.acs.org/journal/acscii

Research Article

Unprecedented Nonphotomediated Hole (h^+) Oxidation System Constructed from Defective Carbon Nanotubes and Superoxides

Junhui Wang, Jiaxing Yu, Qi Fu, Huangsheng Yang, Qing Tong, Zhengping Hao, and Gangfeng Ouyang*

Cite This: *ACS Cent. Sci.* 2021, 7, 355−364

Read Online

ACCESS | Metrics & More | Article Recommendations | Supporting Information

ABSTRACT: Holes (h^+) on heterogeneous photocatalysts could act as important oxidative species or precursors for reactive oxygen species (ROS). However, due to the ultrafast recombination of photoinduced electrons and holes, a majority of carriers are consumed prior to surface reactions. Herein, we report an unprecedented nonphotomediated hole oxidation system constructed from carbon nanotubes (CNTs) and superoxides. This system exhibited high catalytic activity for the degradation of organic pollutants, which outperforms the classical oxidation processes in the remediation of actual wastewater and is comparable to that of the best single cobalt atom catalyst. Theoretical and experimental results reveal that the intrinsic defects with unpaired spins on CNTs served as adsorptive sites to activate superoxides. This is the first report on exploring the oxidation properties of nonphotomediated hole carriers on heterogeneous catalysts, which will be of broad interest for researchers in environmental remediation, chemical synthesis, and biological fields.

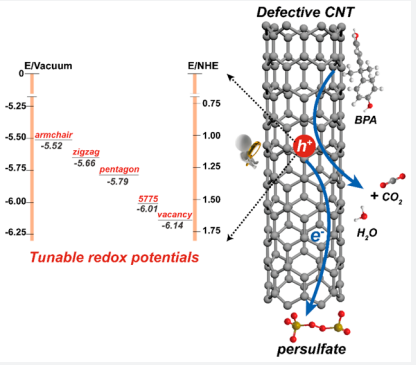

INTRODUCTION

Photoinduced holes (h^+) generated on heterogeneous catalysts could serve as critical active oxidative species in splendid applications, including green energy exploration, chemical synthesis, and environmental technology.[1−3] As the core of photocatalytic activities, the electron−hole separation, transfer, and recombination often take place in an ultrasmall time scale from tens of femtoseconds to hundreds of picoseconds (Scheme 1a),[4,5] which result in the low utilization of photoexcited electrons and holes. For decades, tremendous efforts have been made to increase the separation efficiency of photoexcited electron−hole pairs, via facet/defect engineering or heterojunction construction on the catalysts.[6−9] Even so, still a majority of carriers are consumed by charge recombination prior to surface reactions.[4,10,11]

Considering this, we wonder whether it is possible, through other facile strategies, to trap the electrons and create long-lasting hole carriers with high oxidative potential on the surface of catalysts. Actually, ascribed to the superior electronic conductivity of carbon nanotubes (CNTs), the chemical p-doping by electron-acceptors (e.g., O_2, Br_2) could create hole carriers on CNTs, due to electron transfer from the carbon π states to dopant molecules.[12,13] Most importantly, the hole carriers could exist for at least 5 min during the *in situ* Raman measurements.[12] This feature has offered CNTs exciting opportunities in various electronic/electrochemical applications. However, the oxidative properties of these hole carriers have never been explored.[14,15] Inspired by this observation, we presume that the adsorption of oxidants with strong electron-accepting capability on CNTs might fabricate holes with high oxidative capacity and long lifetime (Scheme 1b).

To increase the adsorption ability of oxidants on CNTs and electron transfer efficiency, more active adsorptive sites should be created. Previous theoretical calculations indicated that the enhancement of the charge or/and spin density of carbon materials could promote catalytic performance due to the increased adsorption affinity of oxidant molecules.[16,17] Recently, the intrinsic defect engineering has been regarded as an effective strategy, including the introduction of zigzag/armchair edges, vacancies, or topological defects (e.g., pentagons, heptagons, and Stone−Wales).[18−23] The defect sites can significantly tailor the surface electronic structures and act as charge-carrier acceptors, which might facilitate oxidant activation by the transfer of the electrons to the adsorbed oxidant molecules.[24,25]

In this work, for the first time, we construct a non-photomediated hole oxidation system via a facile chemical strategy, utilizing defective CNTs and strong electron-accepting superoxides. Persulfate (PS) with a high redox potential ($E^0(S_2O_8^{2-}/SO_4^{2-})$ = 1.96 V_{NHE}) was chosen as the model superoxide in this study.[26] This system exhibited striking catalytic performances for the degradation of organic pollutants (e.g., bisphenol A, BPA), comparable to that of the reported single cobalt atom catalyst. Theoretical and

Received: November 26, 2020
Published: January 11, 2021

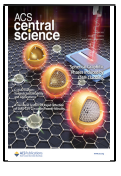

Scheme 1. Design Principle of This Work: Functional Principles of Electron Transfer in (a) Light-Induced Photocatalytic System and (b) Proposed Nonphotomediated Hole Catalytic System. P: Photocatalyst; C: Carbon Nanotube; S: Substrate

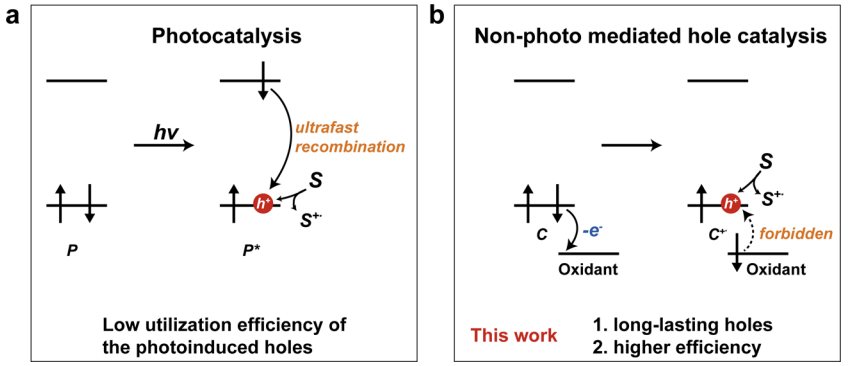

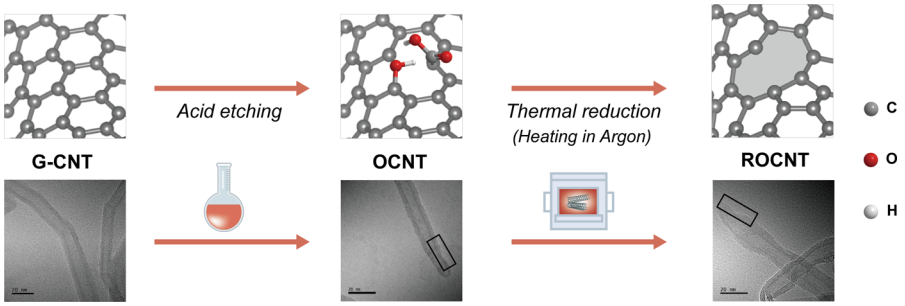

Figure 1. Preparation route and model of defective carbon nanotubes, scale bars: 20 nm.

experimental results verified that the intrinsic defects possess better adsorption affinities for PS and serve as the active sites. Raman, solid UV−vis, electron paramagnetic resonance (EPR), and scavenger experiments confirmed the generation of holes induced by the adsorbed PS on the defect sites and that the holes act as the critical active species for the rapid and selective degradation of BPA in actual wastewater. Intriguingly, the oxidative potentials of the holes could be tuned by proper defect construction on CNTs.

RESULTS AND DISCUSSION

Catalytic Performance of the Defective CNT/PS System. To explore the possible effects of intrinsic defects on PS adsorption and activation, a series of CNTs with different levels of defect exposure were prepared via a facile acid etching and thermal reduction strategy as illustrated in Figure 1. This strategy could regulate the defect contents of CNTs along with maintaining other structural properties almost unchanged. In the acid etching procedure, as shown in TEM images (Figure S1) and reported in ref 27, strong acids could etch the graphene's surface, leading to a higher concentration of edges exposed, and covalently add to its edges and basal planes. And in the thermal reduction procedure, nearly all oxygen/nitrogen-containing functionalities can be desorbed from the CNT lattice by 1000 °C, leading to the formation of zigzag/armchair edges, single vacancy, and pentagon defects.[18,27] Moreover, in CNTs, the Stone−Wales (5775) defect is presumed to be predominant with a relatively low formation energy of 3.5 eV.[27] Therefore, combining the experimental procedure with the intrinsic properties of CNTs, we believe that in the defective CNTs prepared, there mainly existed zigzag edge, armchair edge, pentagon, Stone−Wales (5775), and single vacancy.

In an attempt to further clarify the effect of intrinsic defects on PS adsorption and activation, density functional theory (DFT) calculations were carried out on six CNT theoretical models (Figure S2). Figure 2 shows the local adsorption

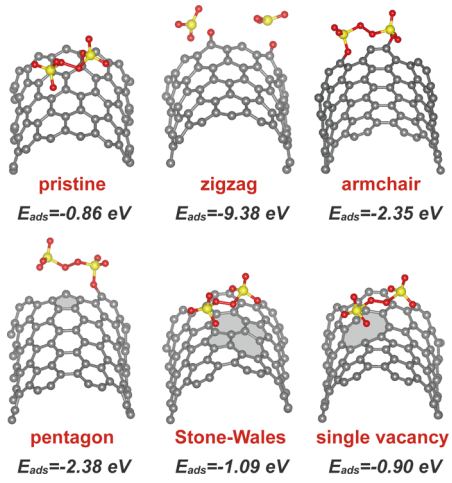

Figure 2. DFT calculations of adsorption affinities of PS on defective CNTs. Local adsorption configurations and adsorption free energies of PS on pristine CNT surface and different kinds of defects on CNT. C gray, O red, S yellow.

configurations and adsorption free energies of PS on a pristine CNT surface and five kinds of defects on the CNT. The results show that all the defect sites possess stronger adsorption for PS molecule (−0.90 to −9.38 eV) than the pristine surface (−0.86 eV). In particular, due to the high adsorption energy, PS could directly dissociate on the zigzag edge. These DFT results reveal that the defects on CNTs possess better chemical activity than

https://dx.doi.org/10.1021/acscentsci.0c01600
ACS Cent. Sci. 2021, 7, 355−364

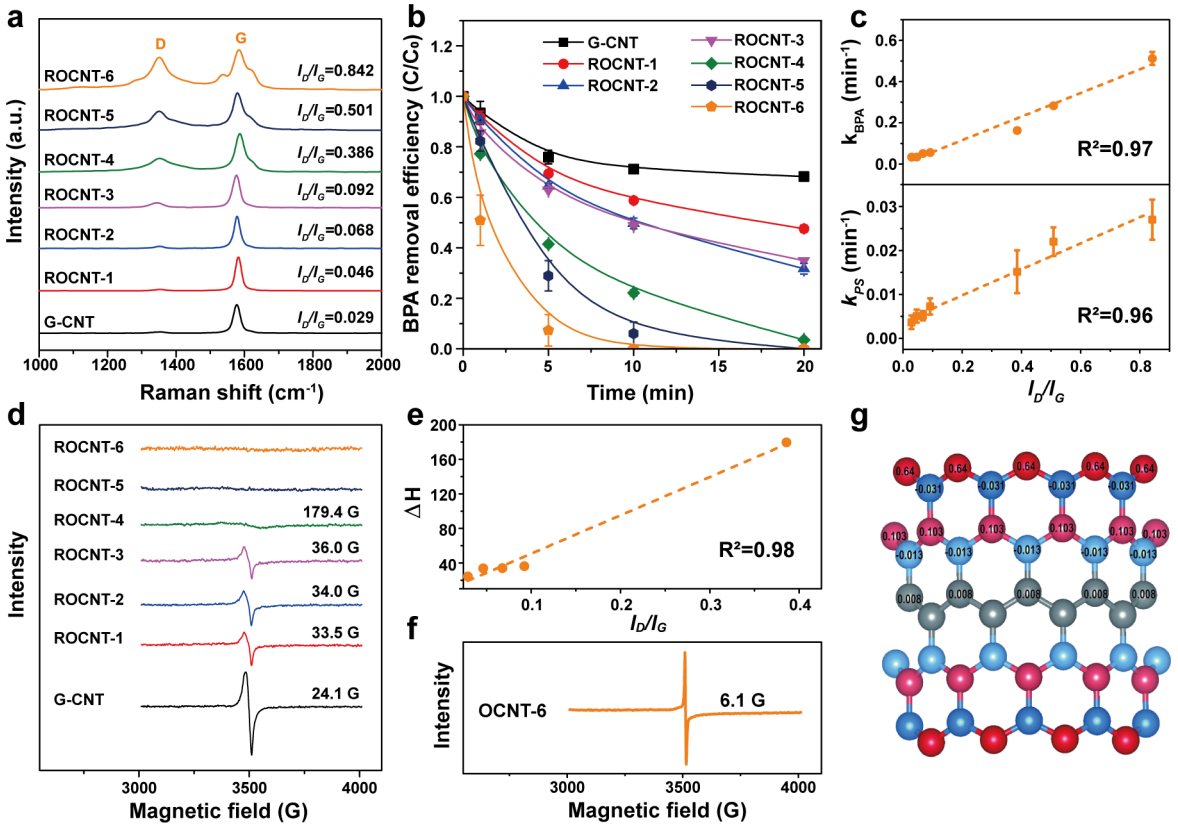

Figure 3. Characterization of defective CNTs and catalytic performance of the CNT/PS system for organic pollutants degradation. (a) Raman spectra of original G-CNT and ROCNTs. (b) Evolution of BPA in different reaction systems catalyzed by G-CNT and ROCNTs. (c) Dependences of k_{BPA} and k_{PS} on the values of I_D/I_G. (d) EPR spectra of G-CNT and ROCNTs. (e) Dependence of line width (ΔH) on the values of I_D/I_G. (f) EPR spectrum of OCNT-6. (g) Spin density distributions on the zigzag edge of CNT obtained from DFT calculations.

the pristine surface and consequently can serve as potential active adsorption sites for PS.

Limited by the available characterization techniques, quantification of different defects in defective carbon materials is still a great challenge.[18,20,27] Therefore, in this study, all the defects in the defective CNTs prepared were treated as a whole and characterized by Raman spectroscopy which is an effective tool to characterize the defects in CNTs.[28,29] As shown in the Raman spectra (Figure 3a), defect levels (the ratio I_D/I_G (D, defect; G, ground)) increased gradually with the acid treatment time. Nitrogen sorption analysis and X-ray photoelectron spectroscopy (XPS) characterization indicated no significant variation of other physical properties (textual structures and heteroatom contents) among the CNTs (Figures S3 and S4 and Table S1). As expected, the catalytic activity for BPA degradation shown in Figure 3b was remarkably enhanced by constructing defects on the CNTs. For instance, in the ROCNT-6/PS system, only 5 min was required for nearly total degradation of BPA. The BPA degradation intermediates were also analyzed and shown in Figure S5. To give a quantitative comparison of the catalytic activities, the BPA degradation kinetics were fitted by the pseudo-first-order model (Figure S6) and the obtained apparent rate constants (k) were listed in Table S1. Further, we correlated the rate constants k_{BPA} to I_D/I_G and found that k_{BPA} presents a positive linear relationship with I_D/I_G and the correlation coefficient (R^2) is as high as 0.97 (Figure 3c). This result indicates that the defects make a crucial contribution to the catalytic activities of CNTs for BPA oxidation. Further investigations were subjected to the catalytic consumptions of PS by the CNTs (Figure S7 and Table S1). Quite similar to the observations above, the PS consumption rate constants (k_{PS}) increased with I_D/I_G and the calculated R^2 reached 0.96, suggesting that it is the defects that act as the active sites for PS adsorption and activation. Furthermore, XPS analyses excluded the possibility of heteroatoms (nitrogen dopants or oxygen-containing functional groups) as the catalytic active sites (Figures S8 and S9). In addition, it is worthwhile to mention that the optimal activity of ROCNT-6, with a k-value of 2.72 μmol/g/s (fitted by a modified kinetic model), is higher than the majority of photo/Fenton-like catalysts recently reported (Table S2) and comparable to that of the single cobalt atom catalyst (3.65 μmol/g/s).[30,31]

Intrinsically, where do the catalytic activities of defects come from? Generally, carbon atoms with larger spin densities are most likely to serve as the active sites.[32,33] To prove this assumption, we performed EPR measurements for different CNT catalysts. As shown in Figure 3d, the EPR spectrum of G-CNT has the narrowest line width (24 G), and those of ROCNTs become broader with the increment of defect levels. The signals are not observable for ROCNT-5 and ROCNT-6, due to the broadening of the signals.[34] The π-electron radical at the defects of CNTs is delocalized to some extent and exhibits fast spin−lattice relaxation through interaction with the adjacent π-electron system, leading to a broad line width in EPR.[32] We also found that the line width ΔH showed a positive correlation with I_D/I_G (R^2 = 0.98) (Figure 3e). To further confirm whether the spin states are important in

https://dx.doi.org/10.1021/acscentsci.0c01600
ACS Cent. Sci. 2021, 7, 355−364

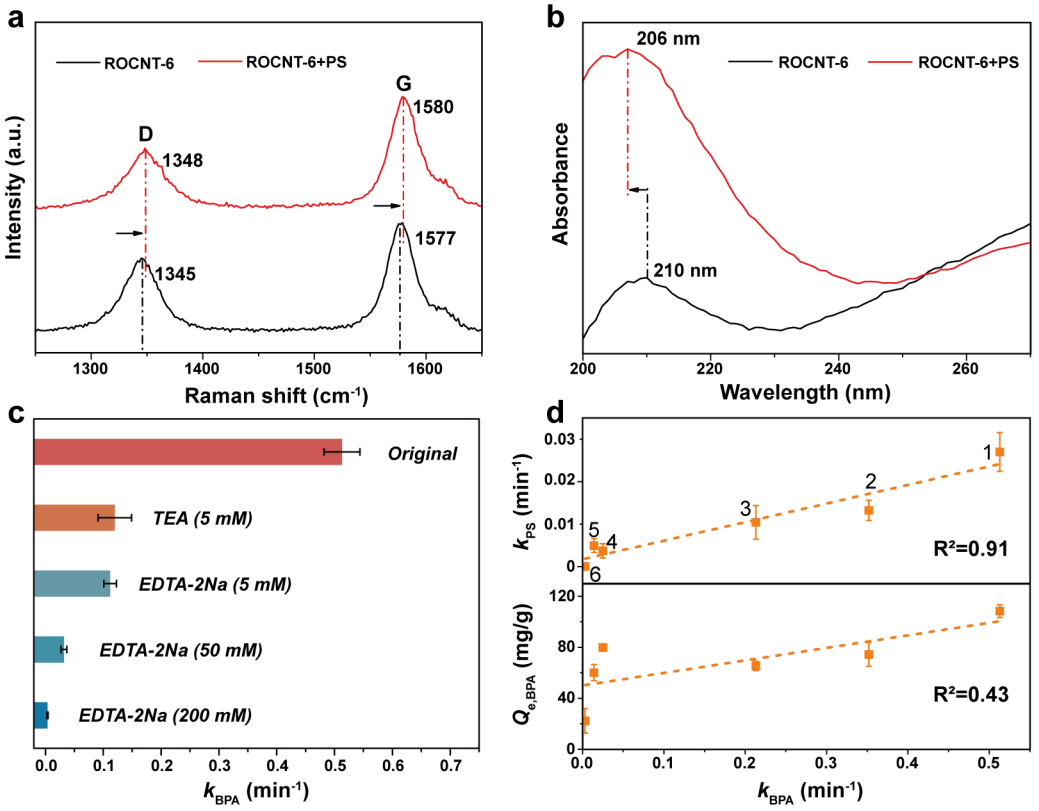

Figure 4. Mechanism investigation of the CNT/PS system. (a) Raman spectra of ROCNT-6 alone and ROCNT-6 adsorbed with PS (b) Solid UV−vis spectra of ROCNT alone and ROCNT adsorbed with PS. (c) Comparison of reaction rates under different quenching conditions. (d) Dependences of k_{PS} and $Q_{e,BPA}$ on the values of k_{BPA} (1. ROCNT-6; 2. NH_2-MWNCT; 3. CON-MWCNT; 4. OH-MWCNT; 5. MWNCT; 6. COOH-MWCNT).

catalysis, OCNT-6 (before the thermal reduction treatment) with intensive carboxyl and hydroxyl groups attached on the defects was measured. Indeed, the EPR peak is quite narrow (6.1 G, Figure 3f), and this is associated with its poor catalytic activity (2.5% BPA removal in 5 min) compared with ROCNT-6 (93% BPA removal in 5 min) (Figure S10). Furthermore, higher spin densities were proved to locate at the zigzag edge by DFT calculation (Figure 3g). Clearly, both the experimental and theoretical results reveal the vital role of unpaired spins at the intrinsic defects in the high catalytic activities of defective CNTs.

Mechanism Investigation. The interaction between the active sites on CNTs and PS molecules was further investigated by Raman, solid UV−vis, and XPS analyses. As shown in Figure 4a, after the adsorption of PS, the characteristic D and G bands at 1345 and 1577 cm^{-1} of ROCNT-6 upshifted by 3 cm^{-1}, indicating that PS serves as an electron acceptor attracting electrons from the carbon π states, consequently creating hole carriers on ROCNT-6.[12,35] Such electronic interaction was also identified by solid UV−vis spectroscopy (Figure 4b). The peak at 210 nm represents the $\pi-\pi^*$ transition of aromatic C−C bonds on ROCNT-6. While after PS adsorption, the absorbance peak downshifted to 206 nm, implying the decrease of electron density on CNT, due to the electron-withdrawing capability of PS.[12] XPS analyses further confirmed that ROCNT-6 could be oxidized by PS if treated for a long time, with oxygen content increased (Figure S11). These results clearly prove the assumption that PS adsorption could cause hole injection into CNTs.

Based on the above observations, quenching experiments were further conducted to identify the active species generated in the CNT/PS system. The commonly used hole scavengers in photocatalysis, triethanolamine (TEA) and ethylenediamine tetraacetic acid disodium (EDTA-2Na), were applied. Not surprisingly, as shown in Figure 4c, TEA and EDTA-2Na both inhibited the BPA degradation effectively, and an increasing amount of EDTA-2Na could induce a higher inhibition effect. Radical quenching experiments and EPR spin-trapping measurements revealed the absence of radicals ($SO_4^{\bullet-}$ or $^{\bullet}OH$) and singlet oxygen ($^1O_2$) during the reaction, which are common active species in traditional oxidation systems, such as photo/Fenton-like reactions (Figure S12). Furthermore, catalytic activities of several commercial MWCNTs were investigated. We observed a positive linear correlation between k_{BPA} and k_{PS} (R^2 = 0.91) rather than the adsorption amount of BPA on CNTs (R^2 = 0.43) (Figure 4d), indicating that the generation of holes induced by PS is the prerequisite for BPA oxidation. If more electrons are extracted by PS, more holes will be generated on CNTs, and higher BPA removal efficiency will eventually be achieved. All of the above observations confirm that holes induced by PS on CNTs were the active species for BPA oxidation.

The reaction process could be further uncovered from the PS consumption under different conditions as illustrated in Figure S13. With only catalyst, the concentration of PS was reduced by 33% in 20 min. In contrast, the presence of electron donors (BPA or EDTA-2Na) led to noticeable decomposition of PS, and the same amount of EDTA-2Na could induce a higher PS consumption rate than BPA, mainly

https://dx.doi.org/10.1021/acscentsci.0c01600
ACS Cent. Sci. 2021, 7, 355−364

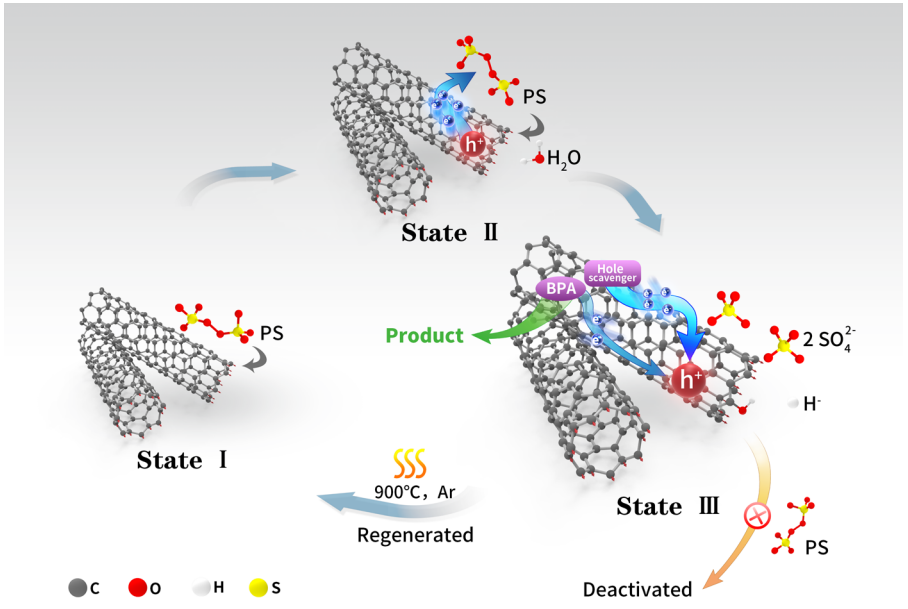

Figure 5. Proposed mechanism of the CNT/PS system. Schematic pathway of defective CNT/PS system for BPA degradation.

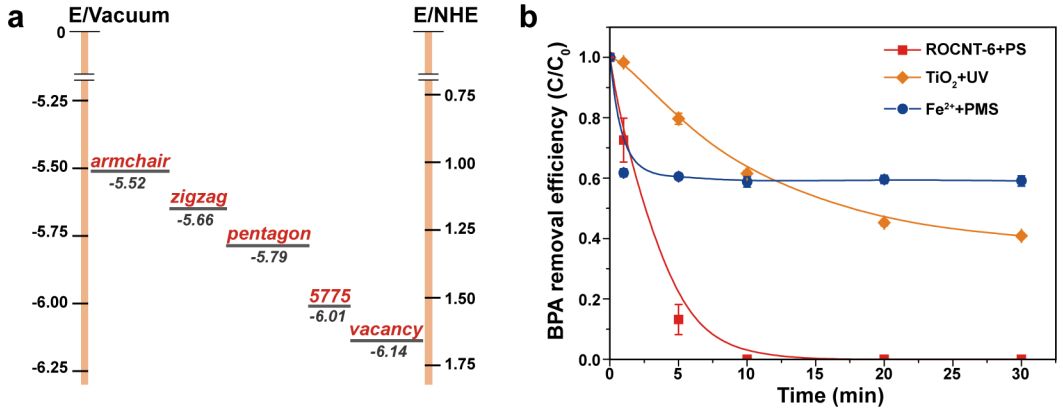

Figure 6. Redox potential investigation of the CNT/PS system. (a) Schematic illustration of the energy diagram for CNTs with PS adsorption on different defect sites obtained from DFT calculations. (b) Catalytic degradation of BPA in the actual water body (Pearl River in China). Reaction conditions: [BPA] = 20 mg/L, [PS] = [PMS] = 1.5 mmol/L, [ROCNT-6] = [TiO_2] = [Fe^{2+}] = 0.1 g/L, T = 298 K.

due to its higher electron-donating capability. These results implied that the electrons from BPA or EDTA-2Na injected to the holes on CNTs could then be transferred to PS leading to its rapid decomposition.

The reusability of ROCNT-6 was also investigated as shown in Figure S14. The used catalyst exhibited reduced activity, and after thermal treatment the catalytic reactivity could be totally recovered. Deactivation was mainly due to the side reaction—oxidation of ROCNT by PS—and the oxygen functionalities could be removed by thermal treatment resulting in the recovery of catalytic activity.

Based on the previous discussions and results, a possible catalytic pathway in the CNT/PS system for BPA degradation is proposed (Figure 5). PS is first adsorbed at the defect sites of CNTs (State *I*) and then extracts unpaired electrons followed by the generation of holes (State *II*). In the meantime, preadsorbed BPA molecules inject electrons into the holes and are oxidized simultaneously. However, if hole scavengers with higher reducibility also adsorb on the CNTs, they are prone to transfer electrons in prior to the BPA molecules, leading to the decrease of BPA degradation rate. Meanwhile, at the defect site, PS is decomposed into two SO_4^{2-} ions, and CNT was oxidized resulting in its deactivation (State *III*). The active sites could be regenerated by removing the oxygen functional groups through thermal treatment in an inert atmosphere.

After understanding the underlying mechanism of this novel oxidation system, we can speculate that other superoxides (e.g., $KHSO_5$, KIO_4, $K_2Cr_2O_7$) could also be applicable, which is verified by experimental data shown in Figure S15. More importantly, as hydrogen peroxide (H_2O_2) is a common oxidant in organisms, the proposed oxidation mechanism might inspire future applications in nanocarbon material-triggered toxicology and therapy.

Redox Potential Investigation of the CNT/PS System. To further identify the oxidation capacities of the holes, DFT calculations were performed to determine the work functions of CNT with PS adsorption on different defect sites. Because the work function is related to the Fermi energy (E_F) of metallic MWCNTs or defined as the HOMO energy of semiconducting CNTs, it could directly reflect the oxidation

https://dx.doi.org/10.1021/acscentsci.0c01600
ACS Cent. Sci. 2021, 7, 355−364

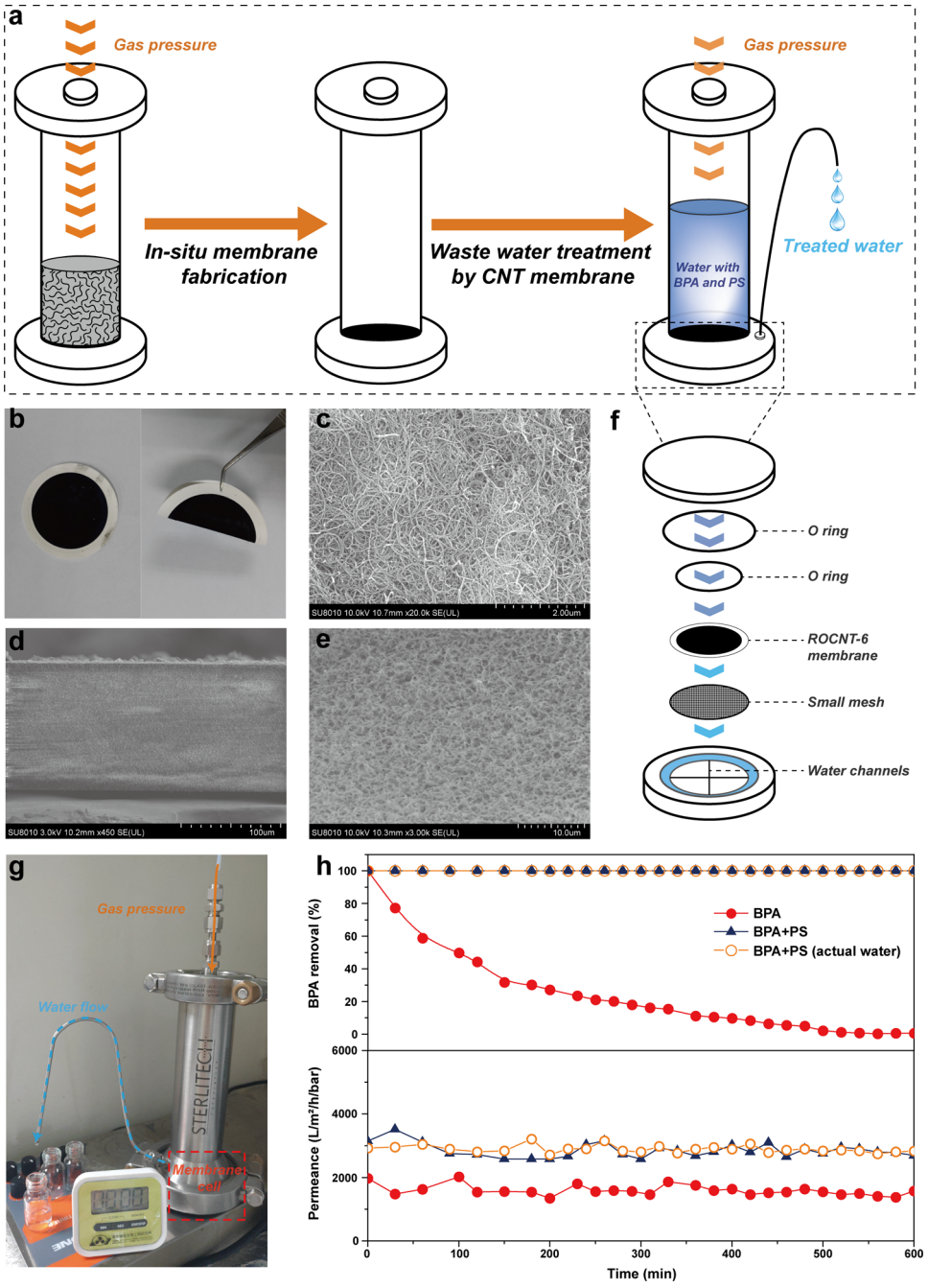

Figure 7. Water treatment in a continuous flow system. (a) Schematic illustration of *in situ* preparation of ROCNT-6 membrane and wastewater treatment process. (b) Photograph of the *in situ* prepared ROCNT-6 membrane with an area of 12.56 cm^2. (c) SEM image of the membrane surface. (d–e) SEM images of the cross-sectional view of the membrane. (f) Schematic representation of the detailed configuration of the membrane cell. (g) Photograph of the experimental setup. (h) BPA removal performance using ROCNT-6 membrane at different conditions. Continuous experimental condition: [BPA] = 2 mg/L, [PS] = 1.5 mM, pH = 7, pressure = 0.1 bar.

potentials of the holes generated on CNTs.[36] For the pristine CNT, the work function is determined as 4.76 eV, in accordance with those reported in the literature.[37,38] When PS adsorbed on the defects of CNT, the work functions increased to 5.66–6.14 eV (shown in Figure 6a), further proving the charge transfer from CNT to PS. The oxidation potentials of the PS-induced holes reflected by work functions are in the range of 1.12 to 1.74 V, indicating that the CNT/PS system possesses moderate oxidation capability. Moreover, from the theoretical calculations, it could be found that the holes generated by PS adsorbed on vacancy and Stone–Wales (5775) defects have more positive oxidation potentials than those on pentagon and zigzag/armchair edges, which indicates that vacancy and Stone–Wales (5775) defects might have better catalytic performances, and the oxidation potentials of this system could be tuned by proper defect construction. The moderate oxidation capability was further confirmed experimentally by the selective degradation of different organic compounds exhibited by the ROCNT-6/PS system (Figure S16). And in the actual water body (detailed water quality parameters shown in Table S3), the catalytic performance of ROCNT-6/PS was scarcely depressed (100% of BPA removal

https://dx.doi.org/10.1021/acscentsci.0c01600
ACS Cent. Sci. 2021, 7, 355–364

in 10 min) (Figure 6b). In comparison, only limited degradation of BPA was obtained by the free radicals produced in the classical Fe^{2+}/peroxymonosulfate (PMS) and TiO_2/UV systems. These exciting results highlight the great efficiency of this novel selective oxidation system for the elimination of target toxic organic contaminants in actual wastewater.

Device Fabrication for Water Treatment in a Continuous Flow System. Due to the rapid degradation of organic compounds in the ROCNT-6/PS system, we further tried to explore its practical application. To avoid the secondary pollution and difficulty of reusing the highly dispersed catalyst suspensions, CNT membranes were fabricated *in situ* simply via filtration of ROCNT-6/water dispersions on a PVDF substrate under gas pressure in a membrane reactor (Figure 7a–b). The SEM images in Figure 7c–e show the random stacking of carbon nanotubes in the membrane with a thickness of about 120 μm and pore size of 200–800 nm. The abundant nanochannels not only provide confined voids for efficient catalytic reaction but also allow fast permeation of the treated water.

After the *in situ* fabrication of CNT membrane, water mixed with BPA and PS was directly added into the membrane reactor, and the following continuous permeance experiments were carried out (Figure 7a, f–g). The removal of BPA in this system maintained 100% over 10 h at a high average permeance of 2850 L/m^2/h/bar (Figure 7h), which is much superior than the best reported MoS_2 membrane (90% BPA removal in 6 h and permeance of 154 L/m^2/h/bar).[30] Waste water containing only BPA was also applied, and leakage of BPA after only 30 min could be observed, implying that the adsorption of BPA by CNTs made negligible contribution to the high removal efficiency. Moreover, the membrane could also maintain its excellent catalytic performance in actual water. We believe that the high catalytic efficiency and nonleakage of any toxic metal ions render this CNT-membrane/PS configuration an ideal oxidation system to selectively remove low-concentration of organic pollutants in actual contaminated water in a continuous flow mode.

In summary, by utilizing defective carbon nanotubes and persulfate, we have fabricated a novel hole oxidation system under dark conditions. This system exhibited striking catalytic performance for the degradation of BPA, and theoretical and experimental results revealed that the intrinsic defects with unpair spins were the active sites for the adsorption and activation of PS. Holes induced by PS at the defects of CNTs were proved to act as the critical active species with moderate and tunable oxidation potentials, rendering the CNT/PS system to have highly efficient and selective elimination toward target pollutants in the actual water body, which could outperform the classical oxidation processes. Furthermore, the optimal CNT catalyst could be fabricated *in situ* into membranes for water treatment in continuous flow. This is the first time to explore the oxidation properties of nonphotomediated hole carriers on heterogeneous catalyst, and the proposed novel oxidation process could offer interesting possibilities for the nonradical selective oxidation in water treatment, chemical synthesis, and biologic applications.

EXPERIMENTAL PROCEDURES

Chemicals and Materials. The following reagents were used as received: G-MWCNT (XF NANO, outer diameter: 10–20 nm, length: 5–30 μm), MWCNT (Aladdin, 95%, inner diameter: 3–5 nm, outer diameter: 8–15 nm, length: 50 μm), NH_2-MWCNT (Aladdin, 95%, inner diameter: 3–5 nm, outer diameter: 8–15 nm, length: 50 μm), OH-MWCNT (J&K, 95%, inner diameter: 5–10 nm, outer diameter: 10–20 nm, length: 10–30 μm), COOH-MWCNT (J&K, 95%, inner diameter: 3–5 nm, outer diameter: 8–15 nm, length: 50 μm), CON-MWCNT (J&K, 95%, inner diameter: 3–5 nm, outer diameter: 8–15 nm, length: 50 μm), potassium peroxydisulfate (Innochem), bisphenol A (Sigma-Aldrich), carbamazepine (Sigma-Aldrich), benzoic acid (Sigma-Aldrich), phenol (Sigma-Aldrich), 4-chlorophenol (Sigma-Aldrich), methanol (Sigma-Aldrich), potassium iodide (Innochem). Ultrapure deionized water (>18 MΩ·cm), produced with a Millipore system, was used for the preparation of all experimental solutions. All chemicals were of reagent grade and were used without further purification or treatment.

Preparation of MWCNTs with Variable Defect Contents. 0.5 g G-CNT was added into a round-bottom flask, followed by slow addition of 120 mL of 68% HNO_3 or 68% HNO_3–98% H_2SO_4 (v/v = 1:3). Then the mixture was magnetically stirred for different periods at 120 °C with refluxing. After cooling down to room temperature, the final mixture was dropped slowly into 500 mL of deionized water under stirring. Then the mixture was filtrated and washed with deionized water until the pH reached ∼7 and was centrifuged at 11000 rmp for 10 min to obtain the solid. Finally, the obtained solid was dried at 120 °C for 24 h and annealed at 1000 °C for 3 h with a heating rate of 3 °C/min under argon atmosphere. The samples treated by HNO_3 for 3 h, 6 h, and 15 h were denoted as ROCNT-1, ROCNT-2, and ROCNT-3, and those treated by couple mixing of HNO_3 and H_2SO_4 for 0.5 h, 1 h, and 1.5 h were denoted as ROCNT-4, ROCNT-5, and ROCNT-6, respectively.

***In Situ* Fabrication of ROCNT-6 Membrane.** 50 mg ROCNT-6 was dispersed in 10 mL Milli-Q water and sonicated for 0.5 h. The ROCNT-6 membrane was then prepared by directly filtering the resultant CNT solution on a PVDF substrate (Millipore) with a pore size of 0.22 μm in the membrane reactor with gas pressure of 0.2 bar. The membrane could be obtained in 30 min.

Characterization. Raman spectra were recorded on a Renishaw InVia spectrometer with a model 100 Ramascope optical fiber instrument. X-ray photoelectron spectroscopic (XPS) analysis was conducted on an ESCALAB 250 spectrometer (Thermo Fisher Scientific Corporation, USA) with Al Kα radiation as the exciting source (150 W). The binding energies of the recorded XPS spectra were corrected according to the C 1s line at 284.8 eV. After subtracting the Shirley-type background, the core-level spectra were deconvoluted into their components with mixed Gaussian–Lorentzian (20:80) shape lines using the CasaXPS software. Brunauer–Emmett–Teller (BET) surface areas were investigated by nitrogen adsorption and desorption at liquid nitrogen temperature (77 K) using a volumetric adsorption analyzer (ASAP2020, Micromeritics Instrument Corporation, USA). The EPR spectra were obtained on a CW/Pulse EPR system (A300, Bruker Co., Germany) with a microwave frequency of 9.64 GHz, a microwave power of 0.94 mW, a modulation frequency of 100 kHz, and a modulation amplitude of 2.0 G. The CNTs were inspected using a high-resolution transmission electron microscope (JEM-2010HR, JEOL, Japan). The concentrations of the ions were detected by an ion chromatograph (Dionex ICS-5000, Thermo Fisher, USA).

https://dx.doi.org/10.1021/acscentsci.0c01600
ACS Cent. Sci. 2021, 7, 355–364

Catalytic Activity Measurements. The entire experiments were performed in 50 mL glass reactors at room temperature. The pH value of the reaction system was not further adjusted and to avoid any misleading conclusions, buffers were not used. The reaction solution was prepared by suspending CNTs (100 mg/L) in the solution of the target organic compound (0.09 mM for all the pollutants). After reaching the adsorption equilibrium, the reaction was initiated by adding an aliquot of a prepared solution of PS (150 mM). Samples were withdrawn using a 1 mL syringe at certain intervals during the 20 min reaction, and the solid was removed by filtration (0.22 μm PTFE filter).

The concentration of PS was measured by a spectrophotometric method using potassium iodide, which was modified from the method suggested by Liang et al.[39] 0.8 mL sample solution was withdrawn and added into a prepared 3 mL KI water solution (containing 0.015 g of $NaHCO_3$ and 0.3 g of KI). The resulting solutions were hand shaken and allowed to equilibrate for 15 min for spectrophotometric measurement at 352 nm.

The concentration of the target organic compounds (i.e., bisphenol A, carbamazepine, phenol, benzoic acid, 4-chlorophenol) was analyzed using a HPLC (Shimadzu LC-20AD). Separation was performed on a Poroshell 120 EC-C18 column (4.6 × 100 mm, 2.7 μm, Agilent Technology, USA) using a mobile phase consisting of a binary mixture of water and methanol at a flow rate of 0.6 mL/min. The degradation intermediates of BPA were identified by direct immersion SPME (solid-phase microextraction) coupled with GC-MS (Agilent 6890-5975 B) equipped with a HP-5 capillary column, using a PA (polyamide) commercial SPEM fiber.

Density Functional Theory (DFT) Calculations. All the calculations are performed in the framework of the density functional theory with the projector augmented plane-wave method, as implemented in the Vienna ab initio simulation package.[40] The generalized gradient approximation proposed by Perdew, Burke, and Ernzerhof is selected for the exchange-correlation potential.[41] The cutoff energy for the plane wave is set to 400 eV. The energy criterion is set to 10^{-5} eV in the iterative solution of the Kohn−Sham equation. The Brillouin zone integration is performed at the Gamma point. All the structures are relaxed until the residual forces on the atoms have declined to less than 0.05 eV/Å. In this work, single wall carbon nanotubes (SWCNTs) are taken as an example to consider the catalytic effect for persulfate adsorption and activation as shown in Figure S1. The simulated carbon nanotube is with a size of $a \times b \times c = 10 \times 10 \times 9.838$ Å and built in a cubic simulation cell with lattice content of 30 Å. The vacuum layer is more than 15 Å along three directions to avoid unphysical interaction between the nanotube and the periodic image because of the periodic boundary condition. To investigate the adsorption affinities of PS molecules on different sites of SWCNTs, the adsorption energy is studied by DFT calculations, defined as

$$E_{ads} = E_{total} - E_{substrate} - E_{molecule}$$

where E_{total}, $E_{substrate}$, and $E_{molecule}$ denote the total energy of substrate with adsorbate, substrate, and free molecule, respectively.

In all experiments performed, no unexpected or unusually high safety hazards were encountered.

■ ASSOCIATED CONTENT

Supporting Information

The Supporting Information is available free of charge at https://pubs.acs.org/doi/10.1021/acscentsci.0c01600.

HRTEM images of G-CNT, ROCNT-3, and ROCNT-6; favorite adsorption configuration of PS on pristine surface and different kinds of defects on CNT; N_2 adsorption−desorption isotherms of CNT catalysts; XPS spectra of CNT catalysts; GC-MS spectra of the BPA degradation intermediates by the ROCNT-6/PS system; kinetic analysis of BPA degradation on different CNT catalysts; PS consumption on different CNTs and the kinetic analysis of PS consumption according to the pseudo-first-order model; high-resolution XPS O 1s and N 1s spectra of the CNT catalysts; contents of different O and N species on the CNT catalysts analyzed from XPS spectra; catalytic degradation of BPA by OCNT-6; XPS spectra and contents of O species of ROCNT-6 and ROCNT-6; variation of $S_2O_8^{2-}$ and SO_4^{2-} ions during the reaction of ROCNT-6/ROCNT-3 with PS solution for 1 h; pH variation during the reaction process under different conditions; EPR spectra obtained by spin trapping with DMPO and TEMP in the presence of PS and ROCNT-6; degradation of BPA by the ROCNT-6/PS system with and without methanol; PS consumption under different conditions; reusability investigation of ROCNT-6; XPS 1Os spectra of used catalyst and regenerated catalyst after 900 °C treatment; catalytic degradation of BPA on ROCNT-6 with other different superoxides adsorbed; catalytic performance of ROCNT-6/PS system for treating different pollutants; physicochemical parameters of the CNTs; comparison of recently reported photo/Fenton-like catalysts in BPA removal; and water quality parameters of Pearl River (PDF)

■ AUTHOR INFORMATION

Corresponding Author

Gangfeng Ouyang − *MOE Key Laboratory of Bioinorganic and Synthetic Chemistry, School of Chemistry, Sun Yat-Sen University, Guangzhou, Guangdong 510275, China; Chemistry College, Center of Advanced Analysis and Gene Sequencing, Zhengzhou University, Zhengzhou 450001, China;* orcid.org/0000-0002-0797-6036; Phone: +86 020 84110845; Email: cesoygf@mail.sysu.edu.cn; Fax: +86 020 84110845/0953

Authors

Junhui Wang − *MOE Key Laboratory of Bioinorganic and Synthetic Chemistry, School of Chemistry, Sun Yat-Sen University, Guangzhou, Guangdong 510275, China;* orcid.org/0000-0001-9022-7417

Jiaxing Yu − *School of Materials Science and Engineering, Sun Yat-Sen University, Guangzhou, Guangdong 510275, China*

Qi Fu − *MOE Key Laboratory of Bioinorganic and Synthetic Chemistry, School of Chemistry, Sun Yat-Sen University, Guangzhou, Guangdong 510275, China*

Huangsheng Yang − *MOE Key Laboratory of Bioinorganic and Synthetic Chemistry, School of Chemistry, Sun Yat-Sen University, Guangzhou, Guangdong 510275, China*

https://dx.doi.org/10.1021/acscentsci.0c01600
ACS Cent. Sci. 2021, 7, 355−364

Qing Tong − *Jiangsu Key Laboratory of Vehicle Emissions Control, Center of Modern Analysis, Nanjing University, Nanjing 210093, China*

Zhengping Hao − *National Engineering Laboratory for VOCs Pollution Control Material & Technology, University of Chinese Academy of Sciences, Beijing 101408, China*

Complete contact information is available at: https://pubs.acs.org/10.1021/acscentsci.0c01600

Author Contributions

J.W. and O.G. conceived the project. J.W., J.Y., Q.F., H.Y. and Q.T. designed, analyzed, and discussed the experimental results. J.Y. and Q.F. carried out the catalytic performance tests. J.W. and H.Y. performed the measurements. Z.H. and O.G. gave suggestions on the experiments and drafted the manuscript.

Notes

The authors declare no competing financial interest.

■ ACKNOWLEDGMENTS

We acknowledge financial support from the projects of the National Natural Science Foundation (Nos. 21806192, 21527813, and 21737006), the Natural Science Foundation of Guangdong Province (2018A030313441), the Fundamental Research Funds for the Central Universities (19lgpy135), and Jiangsu Key Laboratory of Vehicle Emissions Control (OVEC053).

■ REFERENCES

(1) Wolff, C. M.; Frischmann, P. D.; Schulze, M.; Bohn, B. J.; Wein, R.; Livadas, P.; Carlson, M. T.; Jackel, F.; Feldmann, J.; Wurthner, F.; Stolarczyk, J. K. All-in-one visible-light-driven water splitting by combining nanoparticulate and molecular co-catalysts on CdS nanorods. *Nat. Energy* **2018**, *3* (10), 862−869.

(2) Liu, S. W.; Yu, J. G.; Jaroniec, M. Tunable photocatalytic selectivity of hollow TiO_2 microspheres composed of anatase polyhedra with exposed {001} facets. *J. Am. Chem. Soc.* **2010**, *132* (34), 11914−11916.

(3) Koh, M. J.; Khan, R. K. M.; Torker, S.; Yu, M.; Mikus, M. S.; Hoveyda, A. H. High-value alcohols and higher-oxidation-state compounds by catalytic Z-selective cross-metathesis. *Nature* **2015**, *517* (7533), 181−186.

(4) Bai, S.; Jiang, J.; Zhang, Q.; Xiong, Y. J. Steering charge kinetics in photocatalysis: intersection of materials syntheses, characterization techniques and theoretical simulations. *Chem. Soc. Rev.* **2015**, *44* (10), 2893−2939.

(5) Wu, K.; Du, Y.; Tang, H.; Chen, Z.; Lian, T. Efficient extraction of trapped holes from colloidal CdS nanorods. *J. Am. Chem. Soc.* **2015**, *137* (32), 10224−10230.

(6) Wang, H.; Yong, D. Y.; Chen, S. C.; Jiang, S. L.; Zhang, X. D.; Shao, W.; Zhang, Q.; Yan, W. S.; Pan, B. C.; Xie, Y. Oxygen-vacancy-mediated exciton dissociation in BiOBr for boosting charge-carrier-involved molecular oxygen activation. *J. Am. Chem. Soc.* **2018**, *140* (5), 1760−1766.

(7) Kong, M.; Li, Y.; Chen, X.; Tian, T.; Fang, P.; Zheng, F.; Zhao, X. Tuning the relative concentration ratio of bulk defects to surface defects in TiO_2 nanocrystals leads to high photocatalytic efficiency. *J. Am. Chem. Soc.* **2011**, *133* (41), 16414−16417.

(8) Liu, G.; Yang, H. G.; Pan, J.; Yang, Y. Q.; Lu, G. Q.; Cheng, H. M. Titanium dioxide crystals with tailored facets. *Chem. Rev.* **2014**, *114* (19), 9559−9612.

(9) Chen, L.; Furukawa, K.; Gao, J.; Nagai, A.; Nakamura, T.; Dong, Y.; Jiang, D. Photoelectric covalent organic frameworks: Converting open lattices into ordered donor-acceptor heterojunctions. *J. Am. Chem. Soc.* **2014**, *136* (28), 9806−9809.

(10) Kudo, A.; Miseki, Y. Heterogeneous photocatalyst materials for water splitting. *Chem. Soc. Rev.* **2009**, *38* (1), 253−278.

(11) Walter, M. G.; Warren, E. L.; McKone, J. R.; Boettcher, S. W.; Mi, Q.; Santori, E. A.; Lewis, N. S. Solar water splitting cells. *Chem. Rev.* **2010**, *110* (11), 6446−6473.

(12) Rao, A. M.; Eklund, P. C.; Bandow, S.; Thess, A.; Smalley, R. E. Evidence for charge transfer in doped carbon nanotube bundles from Raman scattering. *Nature* **1997**, *388* (6639), 257−259.

(13) Sgobba, V.; Guldi, D. M. Carbon nanotubes-electronic/electrochemical properties and application for nanoelectronics and photonics. *Chem. Soc. Rev.* **2009**, *38* (1), 165−184.

(14) Lee, R. S.; Kim, H. J.; Fischer, J. E.; Thess, A.; Smalley, R. E. Conductivity enhancement in single-walled carbon nanotube bundles doped with K and Br. *Nature* **1997**, *388* (6639), 255−257.

(15) Schroeder, V.; Savagatrup, S.; He, M.; Lin, S.; Swager, T. M. Carbon nanotube chemical sensors. *Chem. Rev.* **2019**, *119* (1), 599−663.

(16) Zhu, J.; Huang, Y.; Mei, W.; Zhao, C.; Zhang, C.; Zhang, J.; Amiinu, I. S.; Mu, S. Effects of intrinsic pentagon defects on electrochemical reactivity of carbon nanomaterials. *Angew. Chem., Int. Ed.* **2019**, *58* (12), 3859−3864.

(17) Tao, L.; Qiao, M.; Jin, R.; Li, Y.; Xiao, Z.; Wang, Y.; Zhang, N.; Xie, C.; He, Q.; Jiang, D.; Yu, G.; Li, Y.; Wang, S. Bridging the surface charge and catalytic activity of a defective carbon electrocatalyst. *Angew. Chem., Int. Ed.* **2019**, *58* (4), 1019−1024.

(18) Jia, Y.; Zhang, L.; Zhuang, L.; Liu, H.; Yan, X.; Wang, X.; Liu, J.; Wang, J.; Zheng, Y.; Xiao, Z.; Taran, E.; Chen, J.; Yang, D.; Zhu, Z.; Wang, S.; Dai, L.; Yao, X. Identification of active sites for acidic oxygen reduction on carbon catalysts with and without nitrogen doping. *Nat. Catal.* **2019**, *2* (8), 688−695.

(19) Shen, A. L.; Zou, Y. Q.; Wang, Q.; Dryfe, R. A. W.; Huang, X. B.; Dou, S.; Dai, L. M.; Wang, S. Y. Oxygen reduction reaction in a droplet on graphite: Direct evidence that the edge is more active than the basal plane. *Angew. Chem., Int. Ed.* **2014**, *53* (40), 10804−10808.

(20) Yan, X.; Jia, Y.; Yao, X. Defects on carbons for electrocatalytic oxygen reduction. *Chem. Soc. Rev.* **2018**, *47* (20), 7628−7658.

(21) Zhang, Y. Q.; Tao, L.; Xie, C.; Wang, D. D.; Zou, Y. Q.; Chen, R.; Wang, Y. Y.; Jia, C. K.; Wang, S. Y. Defect engineering on electrode materials for rechargeable batteries. *Adv. Mater.* **2020**, *32*, 1905923.

(22) Jia, Y.; Zhang, L. Z.; Du, A. J.; Gao, G. P.; Chen, J.; Yan, X. C.; Brown, C. L.; Yao, X. D. Defect Graphene as a trifunctional catalyst for electrochemical reactions. *Adv. Mater.* **2016**, *28* (43), 9532.

(23) Tang, C.; Wang, H. F.; Chen, X.; Li, B. Q.; Hou, T. Z.; Zhang, B. S.; Zhang, Q.; Titirici, M. M.; Wei, F. Topological defects in metal-free nanocarbon for oxygen electrocatalysis. *Adv. Mater.* **2016**, *28* (32), 6845.

(24) Yang, P. J.; Zhuzhang, H. Y.; Wang, R. R.; Lin, W.; Wang, X. C. Carbon vacancies in a melon polymeric matrix promote photocatalytic carbon dioxide conversion. *Angew. Chem., Int. Ed.* **2019**, *58* (4), 1134−1137.

(25) Cheng, Q.; Hu, C.; Wang, G.; Zou, Z.; Yang, H.; Dai, L. Carbon-defect-driven electroless deposition of Pt atomic clusters for highly efficient hydrogen evolution. *J. Am. Chem. Soc.* **2020**, *142* (12), 5594−5601.

(26) Lee, H.; Kim, H.-i.; Weon, S.; Choi, W.; Hwang, Y. S.; Seo, J.; Lee, C.; Kim, J.-H. Activation of persulfates by graphitized nanodiamonds for removal of organic compounds. *Environ. Sci. Technol.* **2016**, *50* (18), 10134−10142.

(27) Collins, P. G. *Defects and disorder in carbon nanotubes*; Oxford University Press, 2010.

(28) Charlier, J. C. Defects in Carbon Nanotubes. *Acc. Chem. Res.* **2002**, *35* (12), 1063−1069.

(29) Fan, Y.; Goldsmith, B. R.; Collins, P. G. Identifying and counting point defects in carbon nanotubes. *Nat. Mater.* **2005**, *4* (12), 906−11.

(30) Chen, Y.; Zhang, G.; Liu, H.; Qu, J. Confining free radicals in close vicinity to contaminants enables ultrafast Fenton-like processes

in the interspacing of MoS_2 membranes. *Angew. Chem.* **2019**, *131* (24), 8218−8222.
(31) Li, X. N.; Huang, X.; Xi, S. B.; Miao, S.; Ding, J.; Cai, W. Z.; Liu, S.; Yang, X. L.; Yang, H. B.; Gao, J. J.; Wang, J. H.; Huang, Y. Q.; Zhang, T.; Liu, B. Single cobalt atoms anchored on porous N-doped graphene with dual reaction sites for efficient Fenton-like catalysis. *J. Am. Chem. Soc.* **2018**, *140* (39), 12469−12475.
(32) Su, C. L.; Acik, M.; Takai, K.; Lu, J.; Hao, S. J.; Zheng, Y.; Wu, P. P.; Bao, Q. L.; Enoki, T.; Chabal, Y. J.; Loh, K. P. Probing the catalytic activity of porous graphene oxide and the origin of this behaviour. *Nat. Commun.* **2012**, *3*, 1298.
(33) Zhang, L.; Xu, Q.; Niu, J.; Xia, Z. Role of lattice defects in catalytic activities of graphene clusters for fuel cells. *Phys. Chem. Chem. Phys.* **2015**, *17* (26), 16733−16743.
(34) Takai, K.; Kumagai, H.; Sato, H.; Enoki, T. Bromine-adsorption-induced change in the electronic and magnetic properties of nanographite network systems. *Phys. Rev. B: Condens. Matter Mater. Phys.* **2006**, *73* (3), No. 035435.
(35) Mo, C. S.; Jian, J. H.; Li, J.; Fang, Z. S.; Zhao, Z.; Yuan, Z. K.; Yang, M. J.; Zhang, Y.; Dai, L. M.; Yu, D. S. Boosting water oxidation on metal-free carbon nanotubes via directional interfacial charge-transfer induced by an adsorbed polyelectrolyte. *Energy Environ. Sci.* **2018**, *11* (12), 3334−3341.
(36) Lim, S. C.; Jeong, H. J.; Kim, K. S.; Lee, I. B.; Bae, D. J.; Lee, Y. H. Extracting independently the work function and field enhancement factor from thermal-field emission of multi-walled carbon nanotube tips. *Carbon* **2005**, *43* (13), 2801−2807.
(37) Ago, H.; Kugler, T.; Cacialli, F.; Salaneck, W. R.; Shaffer, M. S. P.; Windle, A. H.; Friend, R. H. Work functions and surface functional groups of multiwall carbon nanotubes. *J. Phys. Chem. B* **1999**, *103* (38), 8116−8121.
(38) Jiang, B.; Dai, D.; Yao, Y.; Xu, T.; Li, R.; Xie, R.; Chen, L.; Chen, W. The coupling of hemin with persistent free radicals induces a nonradical mechanism for oxidation of pollutants. *Chem. Commun.* **2016**, *52* (61), 9566−9569.
(39) Liang, C.; Huang, C.-F.; Mohanty, N.; Kurakalva, R. M. A rapid spectrophotometric determination of persulfate anion in ISCO. *Chemosphere* **2008**, *73* (9), 1540−1543.
(40) Kresse, G.; Joubert, D. From ultrasoft pseudopotentials to the projector augmented-wave method. *Phys. Rev. B: Condens. Matter Mater. Phys.* **1999**, *59* (3), 1758−1775.
(41) Perdew, J. P.; Burke, K.; Ernzerhof, M. Generalized Gradient Approximation Made Simple. *Phys. Rev. Lett.* **1996**, *77* (18), 3865−3868.

https://dx.doi.org/10.1021/acscentsci.0c01600
ACS Cent. Sci. 2021, 7, 355−364